Supporting Information

Coupling effect between hole storage and interfacial charge transfer over ultrathin CoPi modified hematite photoanode

Pengpeng Wang[a,b], Chunmei Ding[a,b], Dongfeng Li[a,b], Yimeng Cao[a], Zheng Li[a], Xiuli Wang[a,b], Jingying Shi[*a,b], Can Li[*a,b]

[a] *State Key Laboratory of Catalysis, Dalian Institute of Chemical Physics, Chinese Academy of Sciences, Dalian National Laboratory for Clean Energy, Zhongshan Road 457, Dalian 116023, China*
[b] *University of Chinese Academy of Sciences, Beijing 100049, China*

[*]Corresponding author.
E-mail address: jingyingshi@ dicp.ac.cn (J. Shi); canli@dicp.ac.cn (C. Li)

Figures

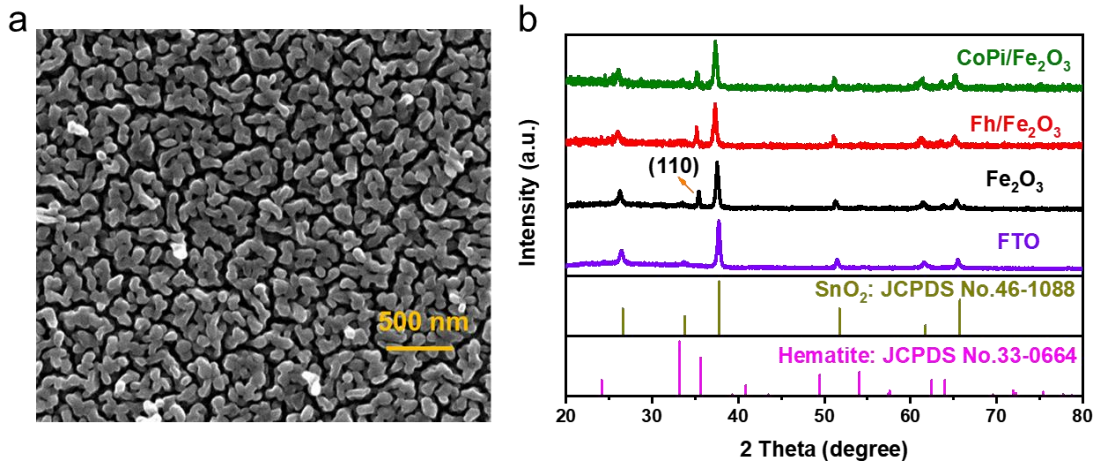

Fig. S1 (a) SEM images of the Fe_2O_3 photoanode. (b) XRD patterns of Fe_2O_3, Fh/Fe_2O_3 and CoPi/Fe_2O_3 photoanodes.

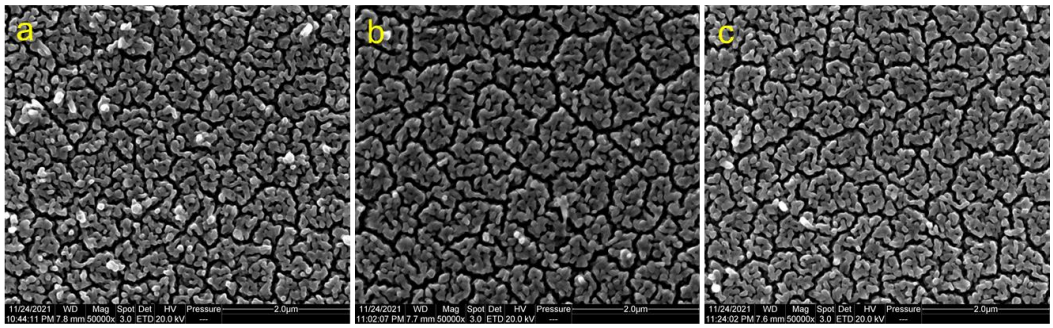

Fig. S2 The SEM images of (a) Fe_2O_3, (b) Fh/Fe_2O_3 and (c) CoPi/Fe_2O_3 photoanodes.

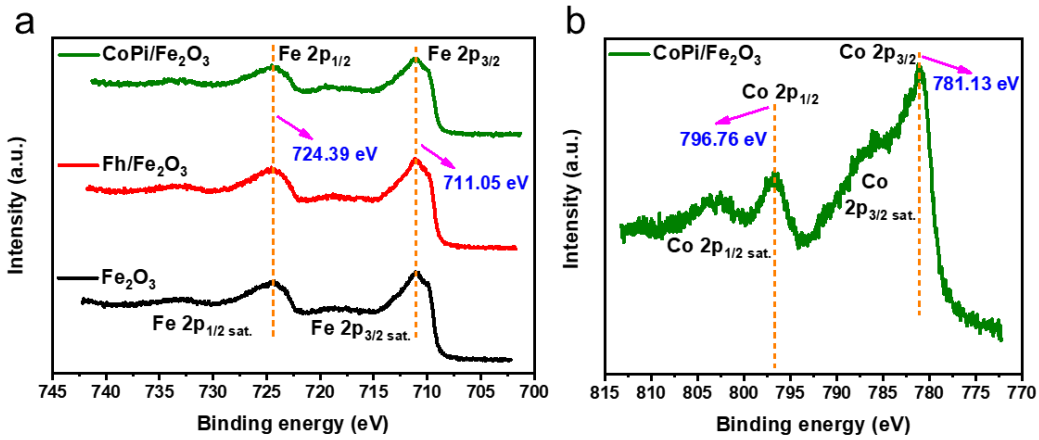

Fig. S3 (a) XPS Fe 2p spectra of the Fe_2O_3, Fh/Fe_2O_3 and $CoPi/Fe_2O_3$ photoanodes. (b) XPS Co 2p spectrum of the $CoPi/Fe_2O_3$ photoanode.

The XPS data for pristine Fe_2O_3 photoanode displayed in Fig. S3a indicate two identical peaks: 724.39 eV of Fe $2p_{1/2}$ and 711.05 eV of Fe $2p_{3/2}$. After ultrathin Fh or CoPi loading, there are little changes for Fe 2p spectra. Meanwhile, the binding energy of 796.76 eV and 781.13 eV in the Co 2p spectrum of $CoPi/Fe_2O_3$ photoanode (Fig. S3b) can be attributed to the presence of Co (II) species.[1, 2]

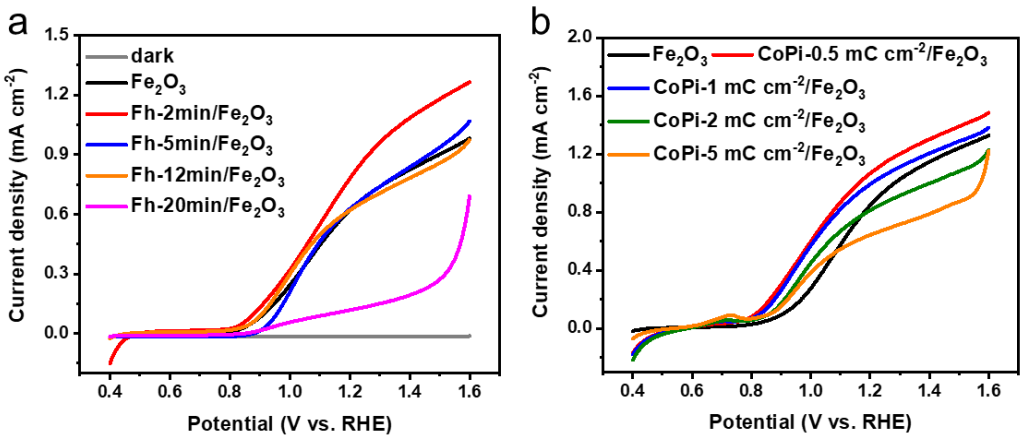

Fig. S4 (a) Current-potential curves of the Fh/Fe_2O_3 photoanodes with different thicknesses of the modified Fh films. (b) Current-potential curves of the CoPi/Fe_2O_3 photoanodes with different thicknesses of the modified CoPi films.

The thicknesses of the Fh and CoPi films decorated on Fe_2O_3 photoanodes were regulated via the deposition time and electric quantity, respectively. The ultrathin Fh film of 2 min and CoPi film of 0.5 mC cm^{-2} were found to possess the highest photocurrent enhancement for Fe_2O_3, respectively.

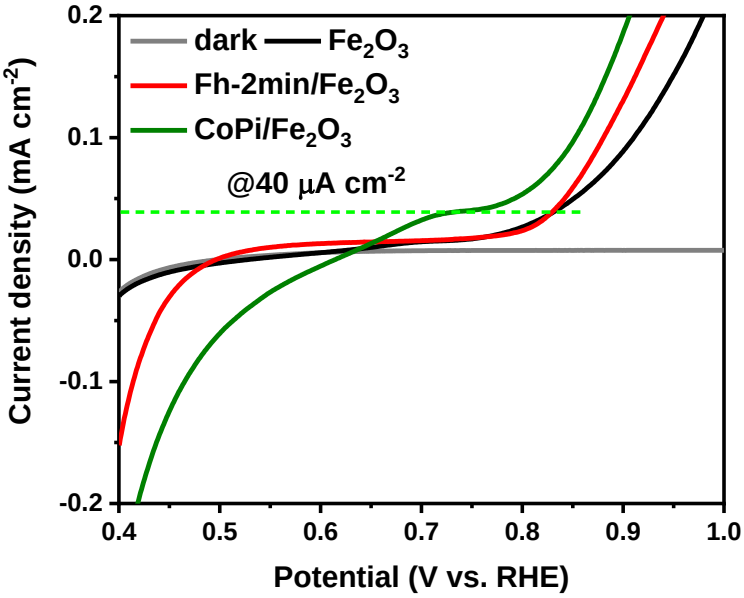

Fig. S5 Current-potential curves of the enlarged images of **Figure 1a** for the studied Fe_2O_3, Fh/Fe_2O_3 and CoPi/Fe_2O_3 photoanodes.

Figure S5 shows that the modification of ultrathin Fh has little effect in photocurrent onset, while the decoration of CoPi can result in 100 mV negative shift of the onset potential.

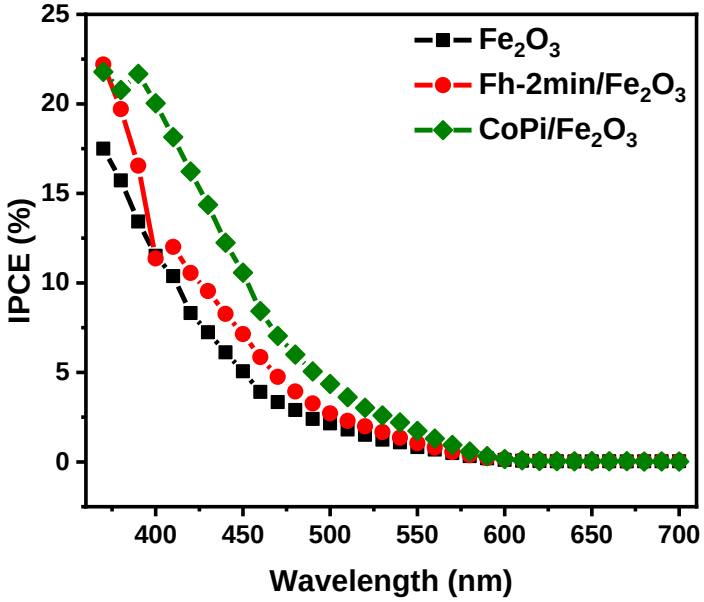

Fig. S6 The IPCE spectra of the studied Fe_2O_3, Fh-2min/Fe_2O_3 and CoPi/Fe_2O_3 photoanodes at 1.23 V *vs.* RHE.

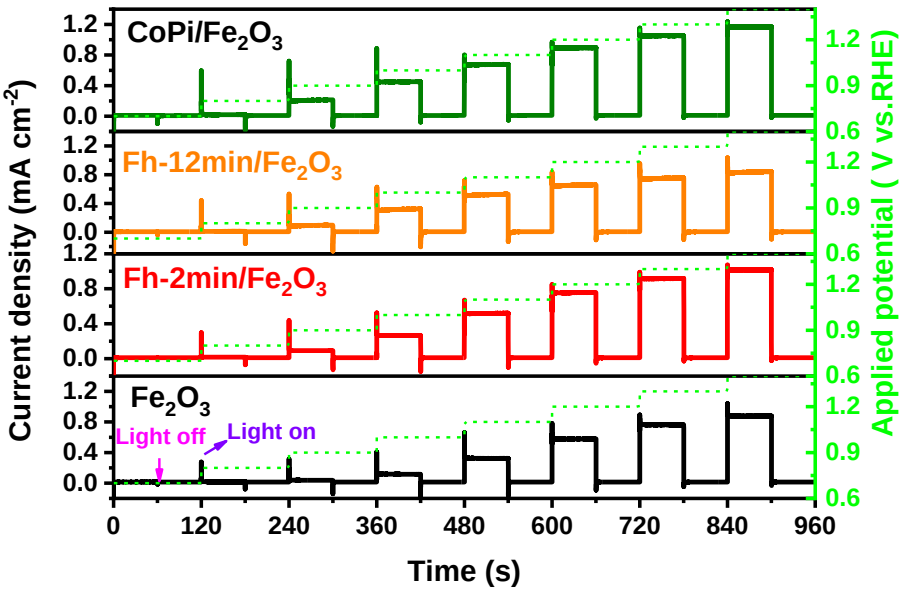

Fig. S7 Chopped light chronoamperometry measurements of the studied Fe_2O_3, Fh/Fe_2O_3 and $CoPi/Fe_2O_3$ photoanodes under AM 1.5 G simulated sunlight (100 mW cm^{-2}) in 1.0 M NaOH solution (pH=13.6). The potential is scanned from 0.70 to 1.40 V *vs.* RHE with 0.1 V step and a 60 s light on/off cycle on each step.

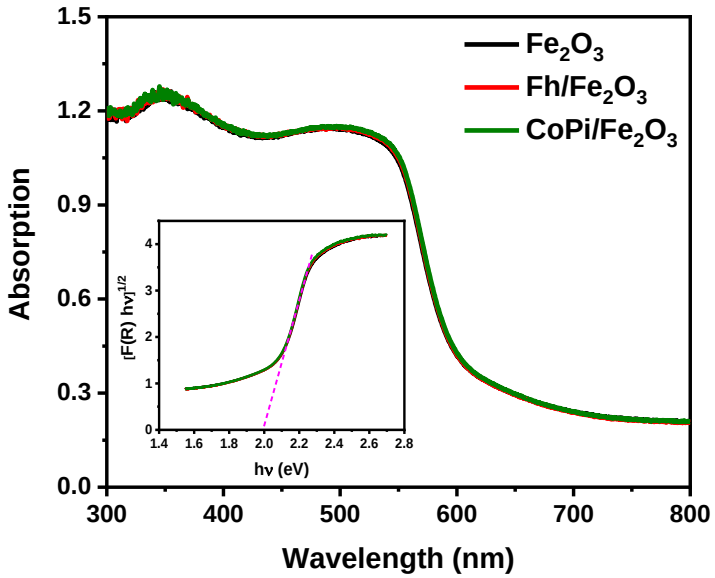

Fig. S8 The UV-visible absorption spectra of the Fe_2O_3, Fh/Fe_2O_3 and $CoPi/Fe_2O_3$ photoanodes. The corresponding band gap (Eg) values were obtained via the Tauc equation and absorption curves, as shown in the insertion graph.

As shown in Fig. S8, the light absorption of the Fe_2O_3 photoanode indicates little changes upon the decoration of Fh or CoPi, thus excluding the possible influences of deposited Fh and CoPi in regulating photocurrent of Fe_2O_3 photoanode.

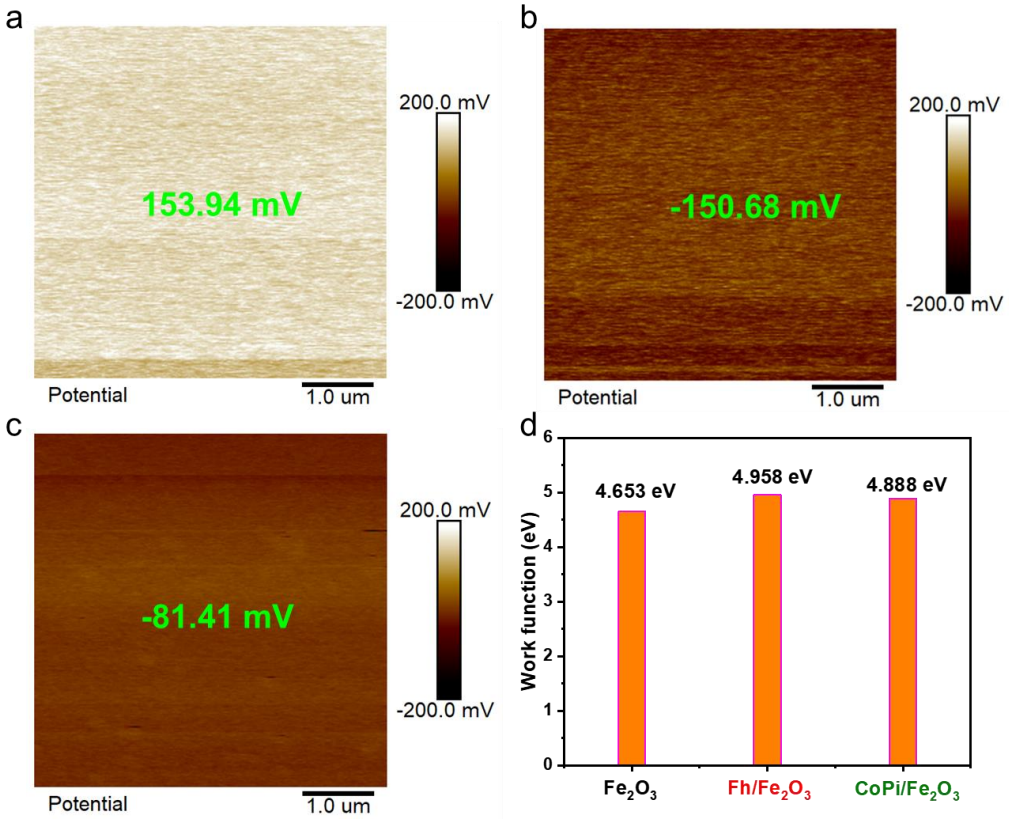

Fig. S9 SKPM images of surface potentials for the studied photoanodes: a) Fe_2O_3; b) Fh/Fe_2O_3; c) $CoPi/Fe_2O_3$; d) The corresponding calculated work functions of the Fe_2O_3 based photoanodes, using HOPG (highly oriented pyrolytic graphite) as the reference.

The surface potential was found to convert from 153.94 mV for bare Fe_2O_3 photoanode to -150.68 mV and -81.41 mV upon the decoration of Fh and CoPi, respectively. These surface potential values may reflect the surface potentials of ultrathin Fh and CoPi themselves. However, the calculated work functions of Fh/Fe_2O_3 and $CoPi/Fe_2O_3$ photoanodes do not demonstrate distinct differences, unveiling that work function is not the factor for influencing the photocurrent improvement.

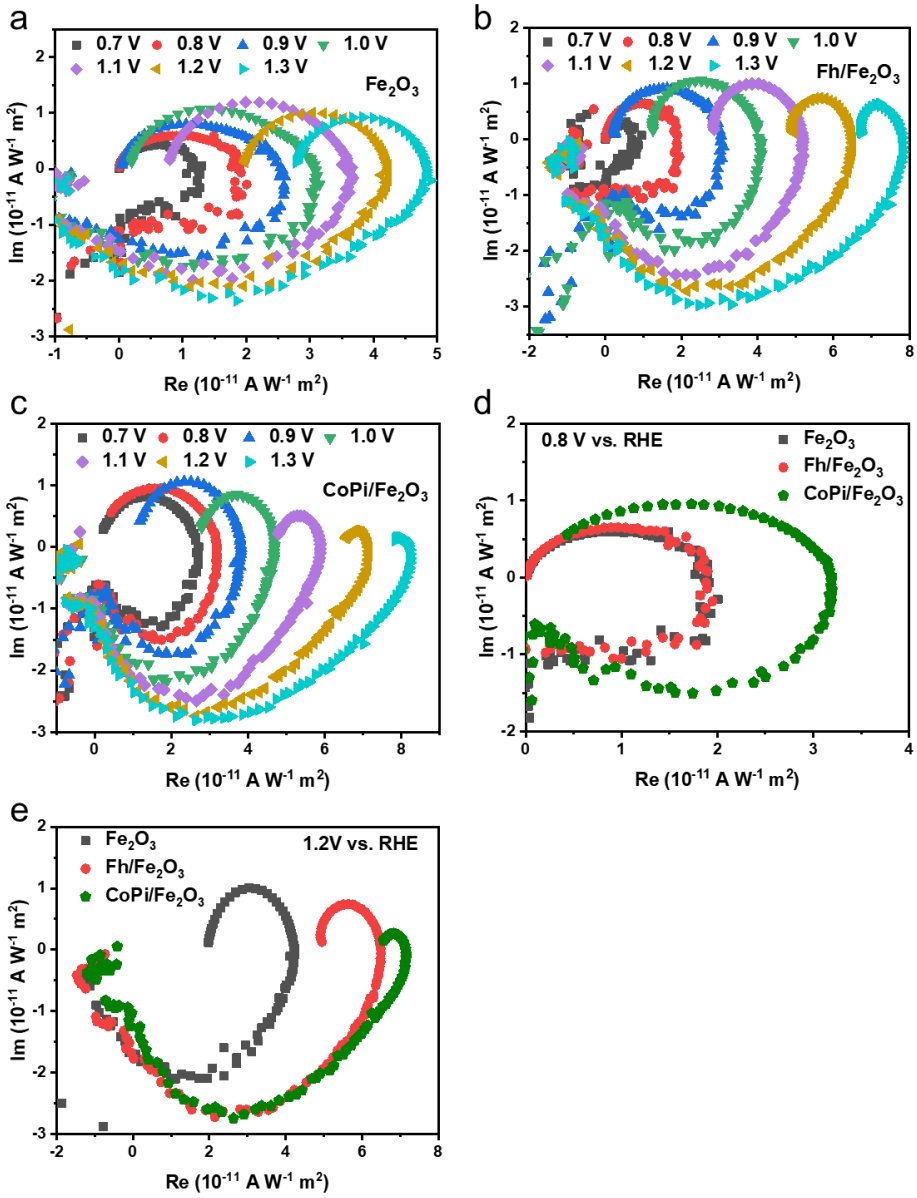

Fig. S10 IMPS spectra of the studied Fe_2O_3, Fh/Fe_2O_3 and CoPi/Fe_2O_3 photoanodes: (a-c) Nyquist curves of the Fe_2O_3, Fh/Fe_2O_3 and CoPi/Fe_2O_3 photoanodes at a series of applied potentials ranging from 0.70 to 1.30 V *vs.* RHE. (d-e) Nyquist curves of the above studied photoanodes at 0.8 V and 1.2 V.

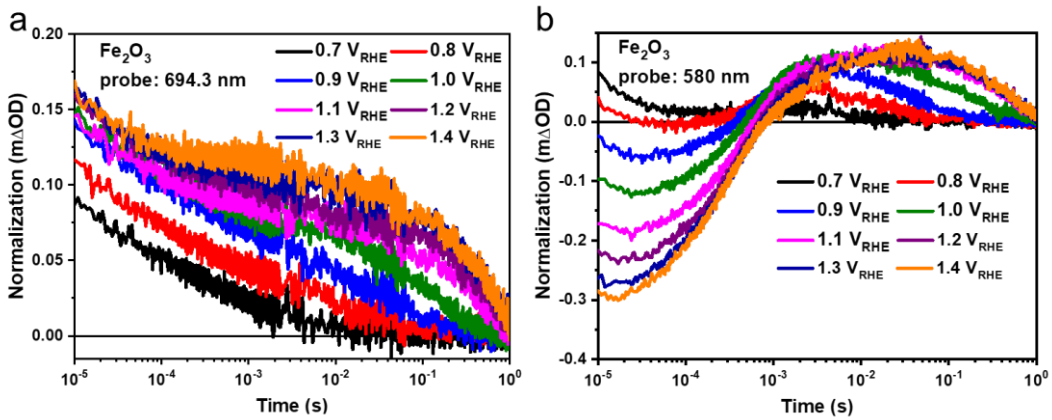

Fig. S11 Bias-dependent transient absorption (TA) spectra of the Fe_2O_3 photoanode under a series of applied bias from 0.7 to 1.4 V *vs.* RHE in 1.0 M NaOH at (a) 694.3 nm and (b) 580 nm.

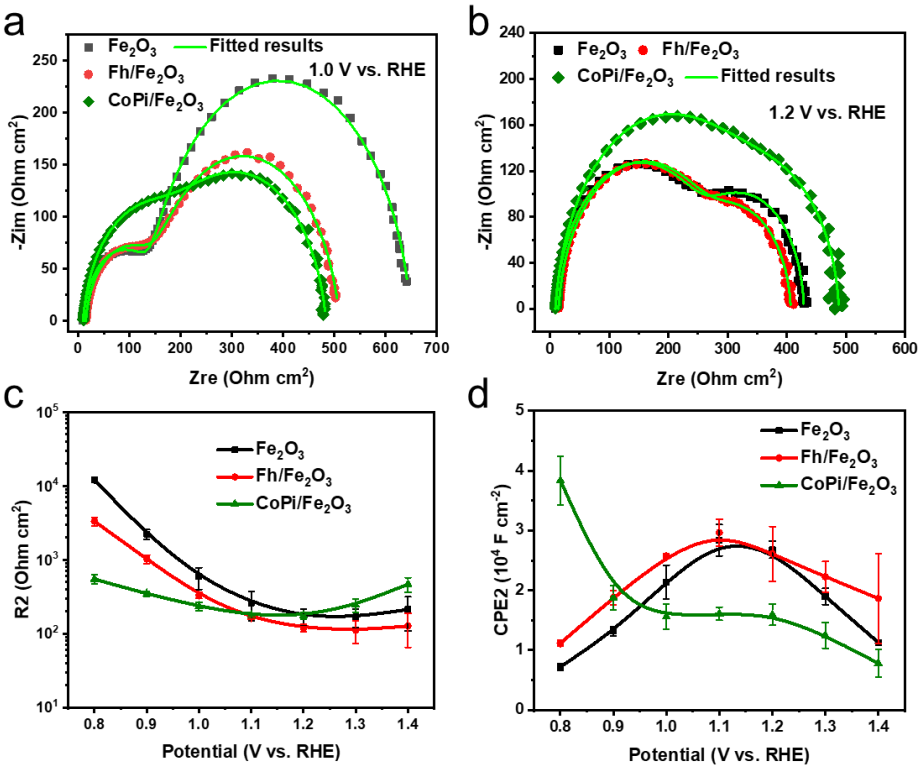

Fig. S12 Electrochemical impedance spectra (EIS) of the studied Fe_2O_3, Fh/Fe_2O_3 and CoPi/Fe_2O_3 photoanodes measured under AM 1.5 G simulated sunlight: (a-b) Nyquist curves of the studied Fe_2O_3 based photoanodes at 1.0 V and 1.2 V *vs.* RHE. (c) The fitted CPE1 versus potential curves. d) The fitted CPE2 versus potential curves.

Fig. S12a and Fig. S12b reflect the electrochemical impedance measurements at 1.0 V and 1.2 V, respectively. The corresponding fitted results are shown in Table S2-3.

It is clearly seen that at 0.8 V, both R1 and R2 indicate gradual decrease upon the decoration of ultrathin Fh and CoPi, demonstrating that the modification of both ultrathin Fh and CoPi layers can result in enhanced bulk charge separation and interfacial injection efficiency. However, at 1.0 V, the R1 values of Fh/Fe_2O_3 and CoPi/Fe_2O_3 photoanodes no longer indicate reduction tendency compared with pristine Fe_2O_3 photoanode. This implies that as the applied potential increasing, bulk

recombination is no longer the dominant factor determining water oxidation and the effect of Fh or CoPi loading in recombination suppression is no longer obvious.

From Fig. S12c, we observed that there are nearly no distinct differences for CPE1 values of Fe_2O_3 and Fh/Fe_2O_3 photoanodes overall the potential region. As for CoPi loading, there are only slight decrease for the CPE1 values of Fe_2O_3 below 1.1 V, which reminds us to further concentrate on the space charge region and band bending changes of Fe_2O_3 upon Fh and CoPi loading.

It is worth noting that there are different behaviors for CPE2 values of Fe_2O_3, Fh/Fe_2O_3 and CoPi/Fe_2O_3 photoanodes, as presented in Fig. S12d. Initially, there are evident increase of CPE2 values for ultrathin Fh or CoPi film modified Fe_2O_3 photoanode at low-potential region. As the potential increasing, however, there are comparable CPE2 values for Fh modified and pristine Fe_2O_3 photoanodes. As for CoPi/Fe_2O_3 photoanode, the CPE2 value demonstrates a rapid decrease in high-potential region, compared with that of pristine or Fh modified Fe_2O_3 photoanode.

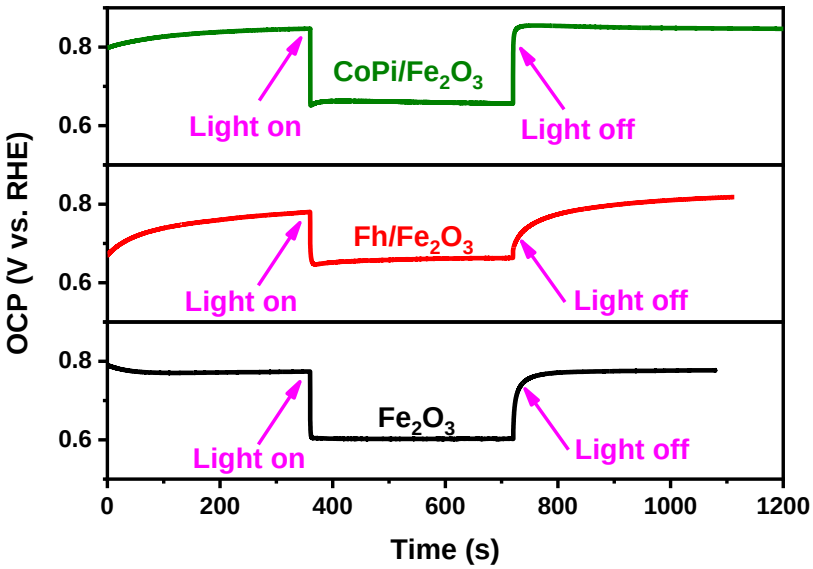

Fig. S13 Open-circuit potential measurements of the studied Fe_2O_3, Fh/Fe_2O_3 and $CoPi/Fe_2O_3$ photoanodes under dark and irradiation conditions. Oxygen was continuously bubbled overall the experiment to maintain the reversible OER at near the standard states.

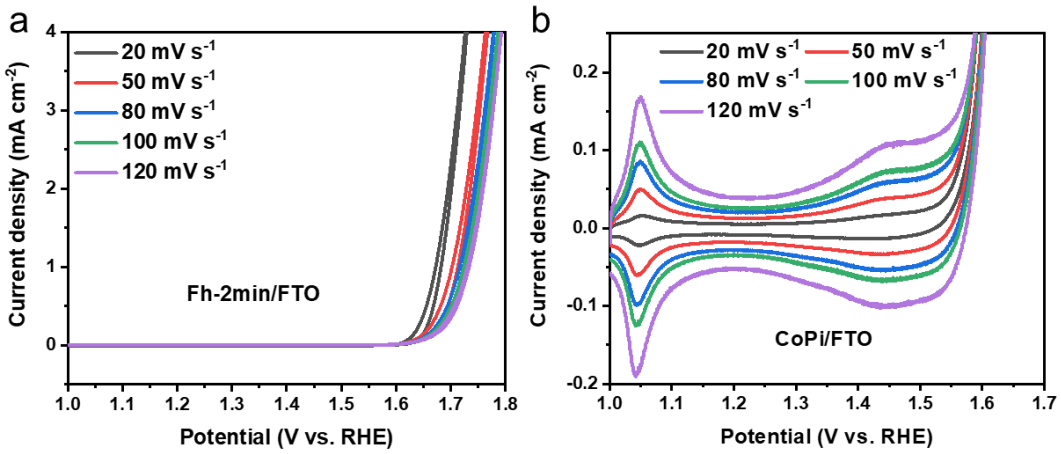

Fig. S14 CV curves of (a) Fh-2min/FTO electrode and (b) CoPi-0.5 mC cm^{-2}/FTO electrode at a series of scan rates under dark condition.

Unlike the characterless CV curves of Fh-2min film (Fig. S14a), it was found from Fig. S14b that there are obvious redox peaks located at 1.05 and 1.45 V *vs.* RHE for CoPi/FTO electrode, which may be ascribed to the processes of Co (II)-Co (III) and Co (III)-Co (IV), respectively.[3]

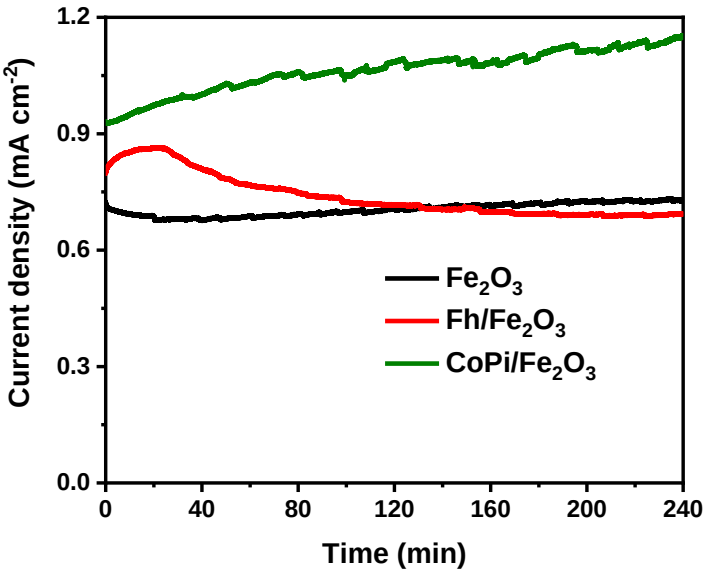

Fig. S15 Chronoamperometry measurements of Fe_2O_3, Fh/Fe_2O_3 and $CoPi/Fe_2O_3$ photoanodes at 1.23 V *vs.* RHE under AM 1.5 G simulated sunlight (100 mW cm^{-2}) in 1.0 M NaOH electrolyte.

Fig. 15 displays the chronoamperometry curves of Fe_2O_3, Fh/Fe_2O_3 and $CoPi/Fe_2O_3$ photoanodes at 1.23 V vs. RHE. The photocurrent of bare Fe_2O_3 electrode slightly decays and then increases a little (<6%), possibly caused by the formation of FeOOH in basic media as the water oxidation cocatalyst.[4]

It is worth noting that upon the decoration of Fh, the photocurrent initially increases within 20 min. Afterwards, the photocurrent decreases and stabilizes at 0.7 mA cm^{-2}, comparable with that of pristine Fe_2O_3. Interestingly, the photocurrent of $CoPi/Fe_2O_3$ increases continuously, from the initial value of 0.98 mA cm^{-2} to 1.15 mA cm^{-2} after 4 h. The phenomenon of initial photocurrent increase can be ascribed to the formation of high-valence species within Fh or CoPi layer during hole extraction and storage process.

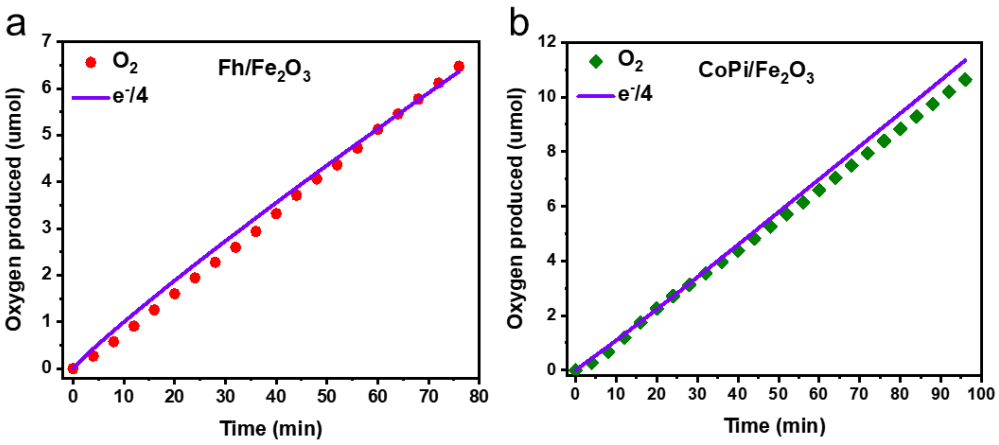

Fig. S16 Oxygen evolution measurement of (a) Fh/Fe_2O_3 and (b) $CoPi/Fe_2O_3$ photoanodes at 1.23 V *vs.* RHE, in comparison with the number of electrons (e^-).

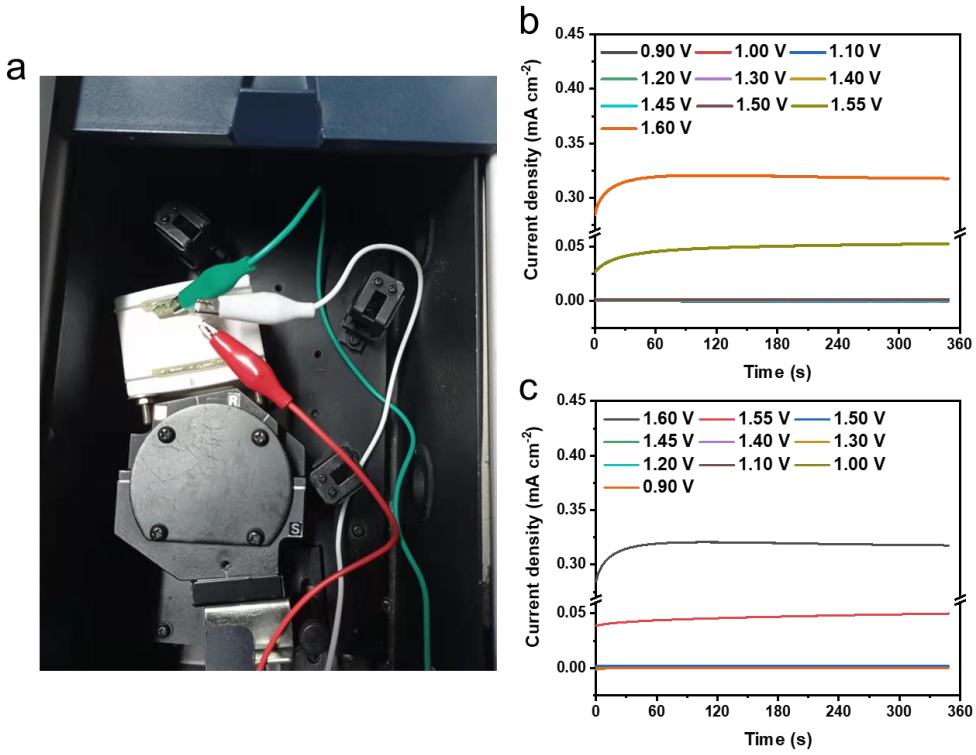

Fig. S17 (a) The image of electrochemical cell placed into the chamber of UV-visible spectrophotometer (JASCO V-550). The CoPi/FTO sample, Pt wire and Ag/AgCl were linked with the CHI 760E electrochemical workstation, which were acted as the working electrode (green wire), counter electrode (red wire) and reference electrode (white wire), respectively; (b) Chronoamperometry measurements of the CoPi/FTO electrode at potentials increasing from 0.90 to 1.60 V *vs.* RHE under dark condition; (c) Chronoamperometry measurements of the CoPi/FTO electrode at potentials decreasing from 1.60 to 0.90 V *vs.* RHE under dark condition.

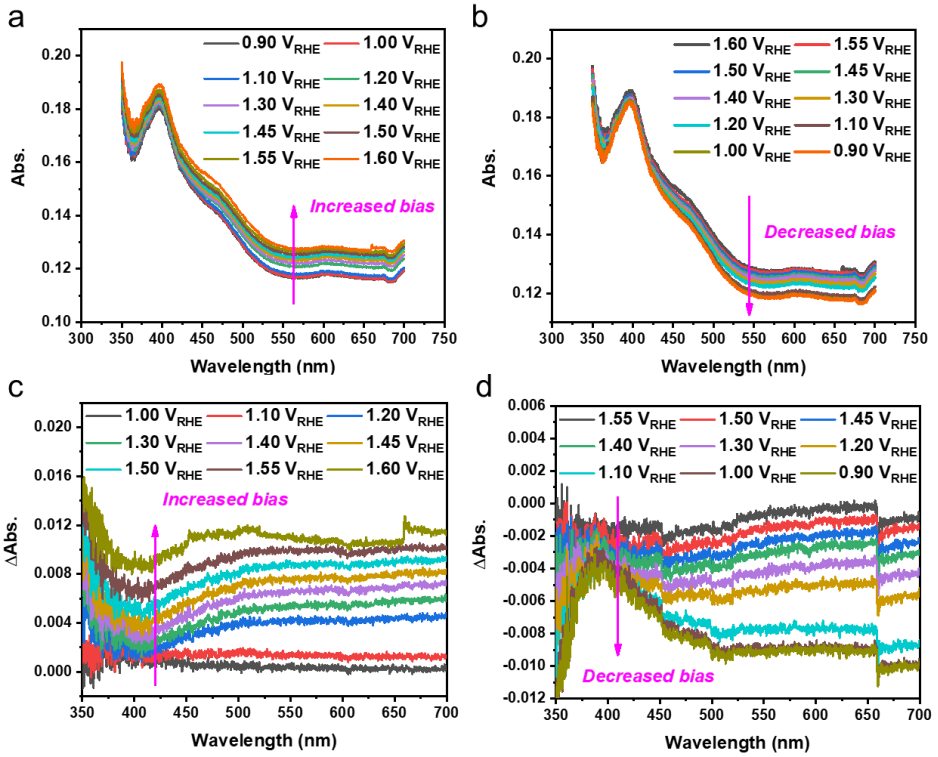

Fig. S18 a) UV-vis spectra of the CoPi/FTO electrode with increasing potential from 0.90 to 1.60 V *vs.* RHE. b) UV-vis spectra of the CoPi/FTO electrode with decreasing potential from 1.60 to 0.90 V *vs.* RHE. c) Changes in the UV-vis spectra of the CoPi/FTO electrode with increasing potential. d) Changes in the UV-vis spectra of the CoPi/FTO electrode with decreasing potential.

Fig. S18 displays the light absorption spectra of CoPi/FTO electrode at continuously increased or decreased potentials and the corresponding differential spectra curves, using the previously reported measurement method.[5] It could be observed that the gradual increased bias results in the arising of well-defined positive absorption, while the reversible negative absorption can be also observed with the bias decreasing.

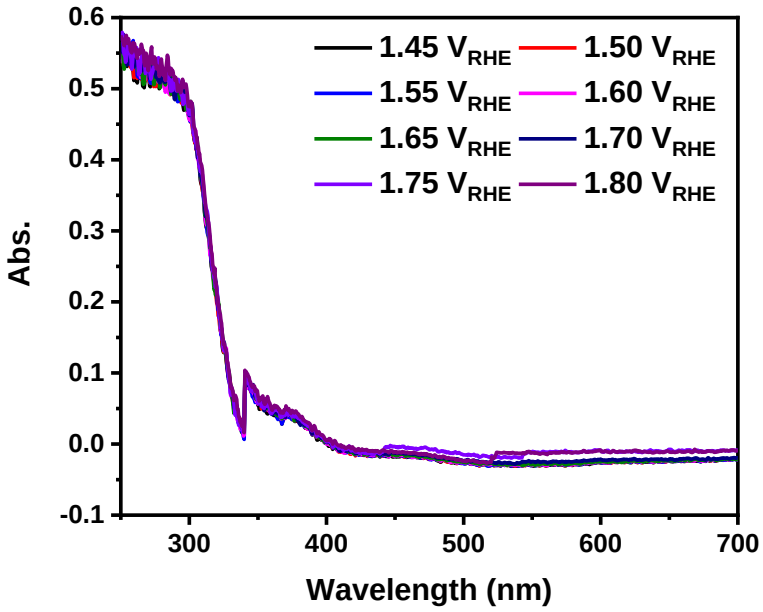

Fig. S19 UV-vis spectra of the Fh/FTO electrode with the increasing potentials from 1.45 to 1.80 V *vs.* RHE.

Table S1. The fitted results of PEIS measured at 0.8 V (*vs.* RHE) in Fig. 3(c).

0.8 V	R1(Ohm cm^2)	R2(Ohm cm^2)	CPE1(10^{-5} F cm^{-2})	CPE2(10^{-5} F cm^{-2})
Fe_2O_3	252.76	12848.16	2.96	7.70
Fh/Fe_2O_3	191.86	3111.97	4.39	10.68
CoPi/ Fe_2O_3	85.65	479.08	2.87	36.52

Table S2. The fitted results of PEIS measured at 1.0 V (*vs.* RHE) in Fig. S12(a).

1.0 V	R1(Ohm cm^2)	R2(Ohm cm^2)	CPE1(10^{-5} F cm^{-2})	CPE2(10^{-5} F cm^{-2})
Fe_2O_3	151.15	490.10	1.93	23.65
Fh/Fe_2O_3	159.05	336.02	2.27	25.86
CoPi/ Fe_2O_3	236.50	237.37	2.03	18.96

Table S3. The fitted results of PEIS measured at 1.2 V (*vs.* RHE) in Fig. S12(b).

1.2 V	R1(Ohm cm^2)	R2(Ohm cm^2)	CPE1(10^{-5} F cm^{-2})	CPE2(10^{-5} F cm^{-2})
Fe_2O_3	279.21	140.59	1.29	25.80
Fh/Fe_2O_3	281.97	110.12	1.42	31.32
CoPi/ Fe_2O_3	366.71	111.59	1.46	22.00

References:

1. M. Oku and K. Hirokawa, *J. Electron Spectroscopy Related Phenomena*, 1976, **8**, 475-481.
2. B. J. Tan, K. J. Klabunde and P. M. A. Sherwood, *J. Am. Chem. Soc.*, 1991, **113**, 855-861.
3. P. Wang, P. Fu, J. Ma, Y. Gao, Z. Li, H. Wang, F. Fan, J. Shi and C. Li, *ACS Catal.*, 2021, **11**, 12736-12744.
4. J. S. Kang, Y. Noh, J. Kim, H. Choi, T. H. Jeon, D. Ahn, J. Y. Kim, S. H. Yu, H. Park, J. H. Yum, W. Choi, D. C. Dunand, H. Choe and Y. E. Sung, *Angew. Chem. Int. Ed.*, 2017, **56**, 6583-6588.
5. A. Li, H. Ooka, N. Bonnet, T. Hayashi, Y. Sun, Q. Jiang, C. Li, H. Han and R. Nakamura, *Angew. Chem. Int. Ed.*, 2019, **58**, 5054-5058.